Energy Advances

ROYAL SOCIETY OF CHEMISTRY

PAPER

View Article Online
View Journal | View Issue

Cite this: *Energy Adv.*, 2024, 3, 2939

n-Doping of bio-inspired electron transporting materials: the influence of charge-transfer complexation†

Wai Kin Yiu, Dylan Wilkinson, Michele Cariello, Marcin Giza, Namrata Pant, Nabeel Mohammed, Benjamin Vella, Stephen Sproules, Graeme Cooke * and Pablo Docampo *

Interest in sustainable and bio-inspired materials for optoelectronic applications is burgeoning, driven by the prospect of greener production, compatibility with large-scale manufacturing and potential biocompatibility. This study introduces two analogues of the biological redox co-factor flavin (**BFG**, **BFA**) as bioinspired electron-transporting materials featuring solubilizing ethylene glycol and alkyl side chains. These materials demonstrated a conductivity of $\sim 5.6 \times 10^{-7}$ S cm^{-1} in their pristine form which compares favourably with widely employed **PCBM** (6.8×10^{-8} S cm^{-1}). To enhance the conductivity of the material the chemical dopant **N-DMBI** was added. UV-vis absorption and electron spin resonance measurements confirmed radical anion formation, while glycol-functionalized derivative **BFG** shows faster reactivity toward the dopant due to increased polarity of the acceptor molecule conferred by the more polar side chain. Surprisingly, these materials did not exhibit the expected enhancement effect in terms of conductivity or increased power conversion efficiency in perovskite solar cells. DFT calculations correlated to features in the absorption spectra of the compounds indicates the formation of stable charge-transfer complexes upon the addition of the dopant. We hypothesise that this inhibits electron transfer of the reduced species in the film to its undoped neighbour and thereby prevents effective doping. Our results highlight the significance of charge-transfer complexation in the design of future electron transporting materials for perovskite solar cells and advocates the use of low cost DFT modelling early on in the design of these species and their dopants.

Received 10th June 2024,
Accepted 2nd October 2024

DOI: 10.1039/d4ya00369a

rsc.li/energy-advances

Introduction

Fullerene based molecules like C60 and [6,6]-phenyl-C61-butyric acid methyl ester (**PCBM**) have found widespread use as electron transporting materials (ETMs) in perovskite solar cells (PSCs) due in part to their excellent electron mobility and good solubility in most organic solvents used in solution processing.[1–3]

Researchers have recently shown a growing interest in the field of green chemistry, utilising cleaner synthetic procedures thereby reducing the negative impact on human health and the environment.[4] The utilisation of biologically-inspired systems and materials could be an alternative route to new materials for solar cells, focusing on the use of relatively non-toxic chemicals and precursors from the natural world.[4] Flavins are biological electron-transporting materials and are excellent candidates for development in this way.[5] In particular, flavins are naturally occurring redox-active molecules that serve as cofactors for enzymes, facilitating various redox reactions and functioning as electron shuttles within metabolic cycles. Synthetic analogues of natural flavins are attractive candidates for the development of new ETMs, due to their convenient synthesis from cheap precursors, inherent stability and convenient electronic tunability by synthetic manipulation.[6]

The optical and redox properties of flavins can be fine-tuned by modifying the phenyl ring (positions C(6)–C(9)), whereas the solubility, and therefore solution processibility, may be modified by varying the nature or the side chains attached to the N(3) and N(10) positions.[7] Flavin derivatives have been used in a number of applications such as in fluorescent probes,[8] photocatalysts[9,10] and batteries.[11,12] Despite the relative ease with which precise adjustments can be made to the properties of flavin derivatives, it is surprising that the photovoltaic properties have only received limited attention.[13]

However, a key stumbling block for developing novel organic semiconductors is their relatively lower conductivity as

School of Chemistry, University of Glasgow, Glasgow, G12 8QQ, UK.
E-mail: Graeme.Cooke@glasgow.ac.uk, Pablo.Docampo@glasgow.ac.uk

† Electronic supplementary information (ESI) available. See DOI: https://doi.org/10.1039/d4ya00369a

compared to inorganic counterparts. This stems from their charge transport mechanism, which relies on hopping between localised molecular orbitals.[14] Additionally, organic semiconductors are susceptible to trap site formation, often caused by disorder and impurities.[15] These factors collectively make the development of novel organic semiconductors challenging.[16] An approach to address low charge transport characteristics is to develop doping approaches employing molecular n-type[17–20] or p-type[21–24] dopants to enhance the conductivity of the materials as well as film morphology,[25,26] and therefore improve the performance of various electronic and optoelectronic devices.[27–34] The interaction between molecular dopants and organic semiconductors relies on charge transfer mechanisms, leading to the formation of radicals and subsequent generation of the free charge carrier within the organic film.[35] In this context, the principle dictates that the LUMO level of p-type molecular dopants should be deeper than the HOMO level of organic semiconductors to generate free holes, whereas the HOMO level of n-type molecular dopants should be shallower than the LUMO of the organic semiconductor to generate free electrons.[25] N-Type doping has been a well-established method to significantly improve the conductivity of **PCBM** derivatives from 10^{-8} S cm^{-1} to 10^{-3} S cm^{-1} by incorporating (4-(1,3-dimethyl-2,3-dihydro-1*H*-benzoimidazol-2-yl)phenyl)dimethylamine (**N-DMBI**).[36–38] This approach has also been successfully applied to PSCs, where it has been shown to boost the power conversion efficiency (PCE) from 16.6% to 18.1%, primarily by improving the short-circuit current density (J_{sc}) and fill factor (FF).[37]

In this study, we report the synthesis of two new flavin analogues with differing solubilizing glycol (**BFG**) and alkyl (**BFA**) side chains (Fig. 1). The alkyl chains were introduced to confer good solubility and thus solution processibility. Moreover, the glycol-based side chain was included to investigate the effect of side-chain polarity on doping efficiency, molecular order, stability and efficiency in resulting devices, a strategy successfully employed for other materials.[39–42] We investigate the optical and redox properties of these systems using UV-vis spectroscopy and cyclic voltammetry, respectively, together with DFT modelling to probe the neutral and reduced states of **BFG** and **BFA**. We also investigate the conductivity of pristine films of these materials and upon doping with **N-DMBI**. Finally, we have fabricated PSCs using **BFG** and **BFA** and report their device parameters.

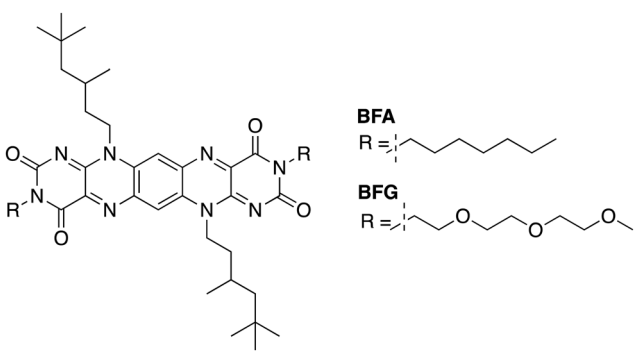

Fig. 1 Structures of **BFA** and **BFG**.

Results and discussions

Synthesis and general characterisation

The synthesis of **BFG** and **BFA** is described in the ESI.† The optical properties of **BFG** and **BFA** were evaluated using UV-vis spectroscopy. Our results indicate that there was no significant influence of side chains on the spectra, as both derivatives exhibited similar absorption profiles as shown in Fig. 2a. Cyclic voltammetry was used to investigate the solution redox properties of **BFG** and **BFA** (Fig. 2b) as well as the dopant, **N-DMBI** (Fig. S10, ESI†). Both NDI derivatives displayed two pseudoreversible reduction waves. By comparing these waves with that of ferrocene (used as internal reference), our results indicate that the two redox waves correspond to two one-electron reductions leading to the radical anion (**BF**/**BF**$^{\bullet-}$) and dianion states (**BF**$^{\bullet-}$/**BF**$^{2\bullet-}$), respectively. The estimated electron affinities (EAs) of **BFG** and **BFA** are −4.17 eV and −4.27 eV, respectively, which are deeper than that of PCBM (−3.92 eV).[43] DFT calculations were performed on an analogue of **BFA** and **BFG** (**BF**) where the alkyl groups were truncated to methyl units to facilitate the calculations (see ESI†). The gas phase HOMO and LUMO energies were calculated to be −6.70 and −4.07 eV, respectively (Fig. 2c). This suggests that **BFG** and **BFA** are in the appropriate range to serve as effective electron acceptors for PSCs.[44–46]

Doping experiments

To enhance the conductivity of the developed materials, (4-(1,3-dimethyl-2,3-dihydro-1*H*-benzoimidazol-2-yl)phenyl)dimethylamine (**N-DMBI**) was employed as the n-type dopant. **N-DMBI** is well-documented for its effectiveness in catalysing the reductive transformation of organic materials[47] and forming radical species in electron transfer reactions.[48,49] The HOMO level of **N-DMBI** is −4.67 eV, which is lower than **PCBM**, **BFG** and **BFA**. Therefore, electron transfer cannot typically occur directly between **N-DMBI** and **BFG** or **BFA** due to energy level misalignment.[47,50,51] The singly occupied molecular orbital (SOMO) depicted in Fig. 1c is associated with **N-DMBI** radical. This radical forms upon activation of the compound through photo[51] or thermal processes,[51,52] which induces hydride transfer. The SOMO of the **N-DMBI** radical is positioned at −2.36 eV,[47] suggesting that it can participate in electron transfer to the flavin derivatives.

To gain the insights into the doping impact on **BFA** and **BFG**, we conducted a series of experiments focused on assessing the influence of **N-DMBI** concentration and reaction times using UV-vis absorption measurements (Fig. 3 and Fig. S11, S12, ESI†). Upon addition of the dopant and application of heat, our results clearly show the appearance of a new peak at 675 nm for both synthesised analogues, as shown in Fig. 3a and b. This indicates the formation of a charged species.[53] This is a result of the action of the chemical dopant, as the peak increases in intensity with increasing **N-DMBI** concentration.

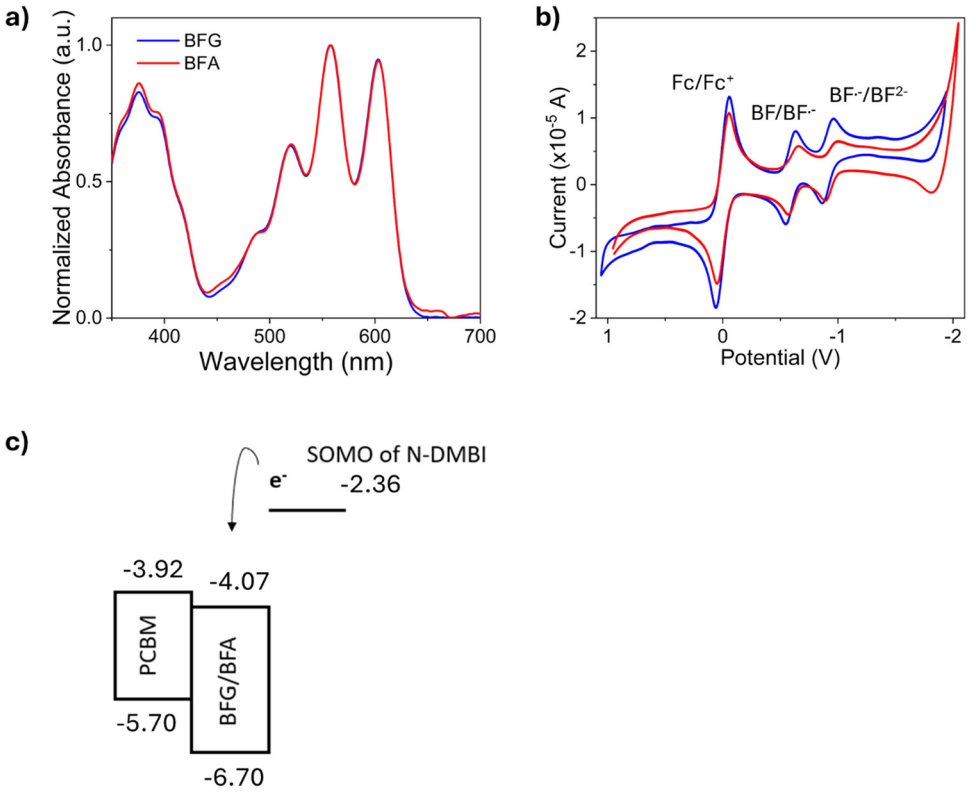

Fig. 2 (a) Solution UV-vis spectra of **BFG** and **BFA** in chlorobenzene (1×10^{-5} M); (b) cyclic voltammetry measurements of **BFG** and **BFA** with ferrocene as the reference ($\sim 8 \times 10^{-4}$ M in CH_2Cl_2; scan rate 100 mV s^{-1}), a wide potential window selected to ensure all redox processes are captured; and (c) energy levels of **PCBM**, **BFG**, **BFA** and **N-DMBI** (HOMO/LUMO of **BFG** and **BFA** from DFT calculations of **BF**).

To ensure that the dopant has fully reacted, a 100 mol% **N-DMBI** concentration was added (Fig. 3c and d) over a 24-hour period under gentle heat of 70 °C. Heating is necessary to fully activate the doping process for this type of molecule.[47] The peaks at 675 nm appeared at 2 hours into the reaction, indicating the formation of a charged species. Interestingly, the peaks for **BFG** and **BFA** showed slightly different progression, with the peak for **BFG** reaching its maximum at 3 hours of reaction, while **BFA** took 6 hours to reach its maximum. This observation suggests that the glycol-modification in **BFG** accelerates the formation of the charged species as compared to **BFA**. This is expected since the glycol moiety provides a polar environment that improves the miscibility and interactions between the ETM and dopant.

To confirm the nature of the formed species, we conducted electron spin resonance (ESR) measurements. Upon the addition of 20 mol% **N-DMBI** to both acceptors, a strong paramagnetic signal with a *g* value of 2.003 was observed, indicating the formation of radical anions. In contrast, no appreciable radical signal was detected in the undoped **BFG** and **BFA** samples (Fig. 3e and f). The enhanced ESR signal in doped **BFG** and **BFA** suggests a higher concentration of anion radicals, which can be attributed to electron transfer from **N-DMBI** to both acceptors. However, it is important to note that UV-vis spectroscopy indicated that the radical anion of **BFG** is more stable than **BFA**. After 24 hours, UV-vis spectroscopy showed that the intensity of the peak at 675 nm for **BFG** remained largely unchanged, whereas the intensity of this peak for **BFA** dropped to a lower level over this time period. These findings highlight the relationship between the molecular side chain, reaction kinetics, and stability, underlining the importance of side chain choice in the doping process.

Conductivity measurements

To verify the suitability as electron transporting materials for solar cells the conductivity of films deposited on patterned-ITO was determined. The conductivity was extracted from the resistance values of standard current–voltage curves employing an interdigitated electrode pattern, as shown in Fig. 4a. The results showed that both **BFG** and **BFA** exhibited similar conductivity values of $\sim 5.6 \times 10^{-7}$ S cm^{-1}, which is an order of magnitude higher than **PCBM** with conductivity values in the range of 6.75×10^{-8} S cm^{-1} (measured in our laboratory), which is consistent with other reports in literature.[17,36,54] In combination with their suitable HOMO/LUMO energy levels, this suggests that **BFA** and **BFG** derivatives have the potential to serve as electron transport layers in optoelectronic devices.

To confirm the radical formation in the film, solid-state UV-vis absorption measurements were performed on undoped and doped flavin derivatives. A concentration of 20 mol% **N-DMBI** was selected to perform these experiments as our solution data (Fig. 3) shows significant radical anion formation. Similarly to the results in solution, the absorption spectrum of thin films deposited *via* spin coating (see Experimental section) showed the formation of new peaks at 690 and 1019 nm for **BFG** and

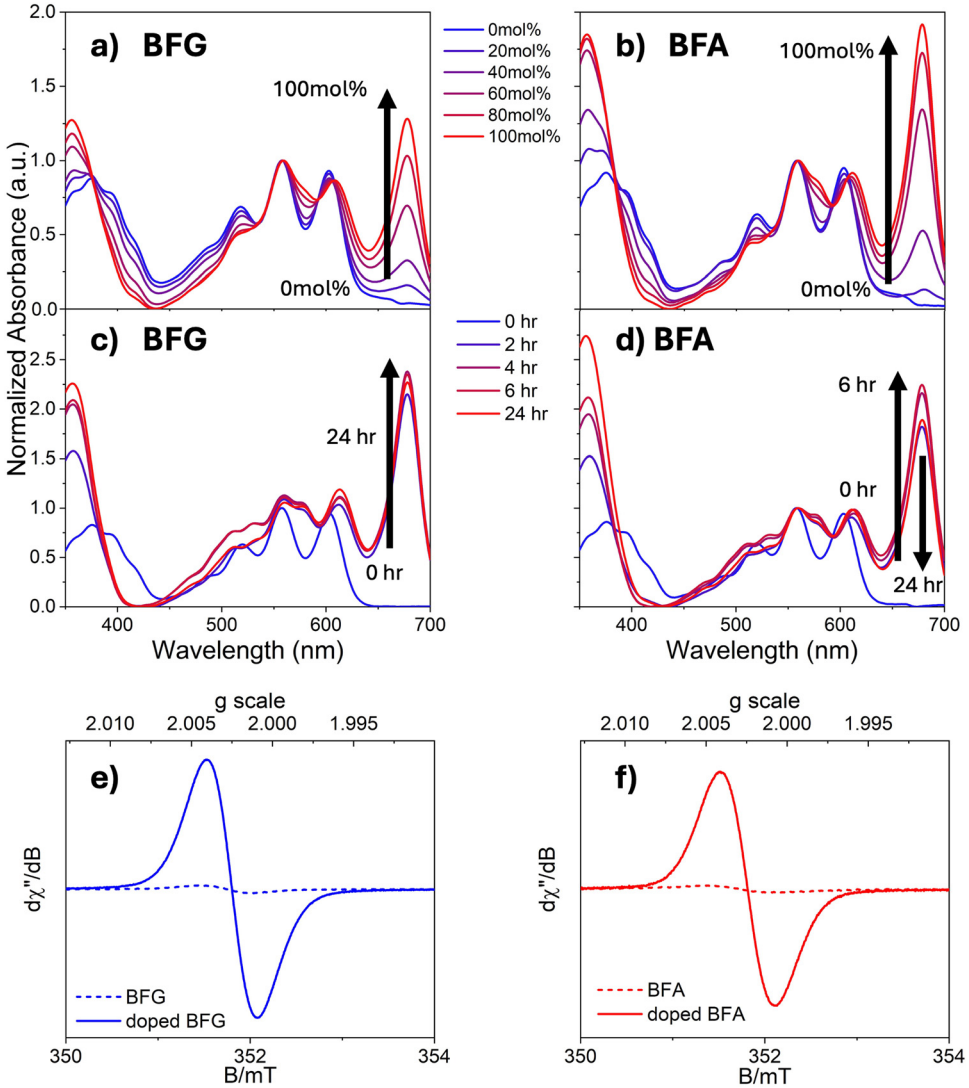

Fig. 3 UV-vis absorption spectra of (a) **BFG** (1×10^{-5} M) and (b) **BFA** (1×10^{-5} M). Spectra of (c) **BFG** and (d) **BFA** recorded in the presence of 0 mol% to 100 mol% **N-DMBI** with reaction times ranging from 0 to 24 hours. The absorption spectra were normalized at 558 nm. X-Band EPR spectrum of undoped and **N-DMBI** doped (e) **BFG** and (f) **BFA** recorded in chlorobenzene ($\sim 2 \times 10^{-2}$ M).

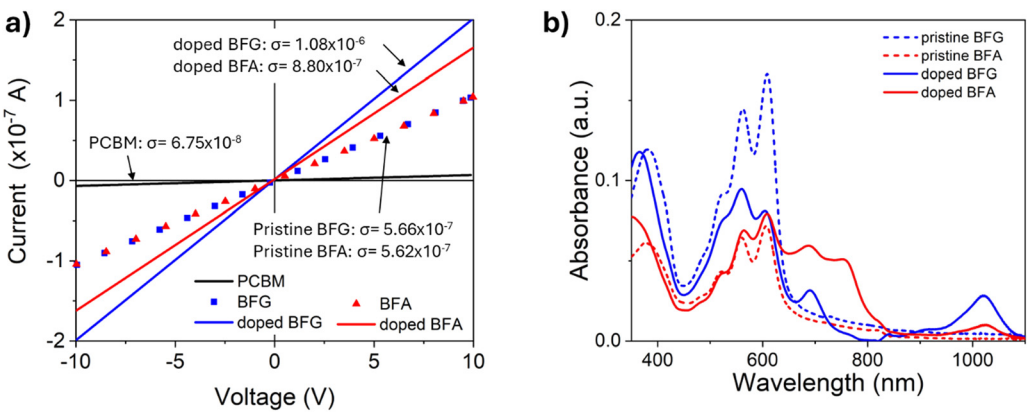

Fig. 4 (a) Conductivity measurement of undoped and 20 mol% of **N-DMBI** doped **BFG** and **BFA**; (b) solid state UV-vis absorption spectra of undoped and 20 mol% of **N-DMBI** doped **BFG** and **BFA**.

687 and 1023 nm for **BFA** (Fig. 4b). These new peaks are consistent with those observed in solution. The broadness of these peaks might be influenced by packing effects induced by the dopants, as suggested by scanning electron microscopy (SEM) (discussed later). The variations in absorption peaks are mainly attributed to differences in film quality as a result of the spin coating process. However, it is worth noting that the conductivities of **BFG** and **BFA** did not show significant improvement after doping from 5.6×10^{-7} S cm^{-1} for the pristine ETM to 1.08×10^{-6} S cm^{-1} of **BFG** and 8.80×10^{-7} S cm^{-1} for **BFA** (Fig. 4a). This result is unexpected, as increases in conductivity of several orders of magnitude are routinely obtained with the addition of chemical dopants when employing state-of-the-art organic semiconductors[55–57] and suggests that the radical species formed in the films are not able to donate the additional electron into the matrix.

Photovoltaic performance in PSCs

To evaluate the potential of flavin derivatives as ETMs in devices, solar cells were fabricated with a standard configuration of glass/ITO/MeO-2PACz/Al_2O_3 NPs/perovskite/ETL/BCP/Ag. The behaviour of **BFA** and **BFG** based perovskite solar cells was compared to that of **PCBM**-based cells. In Fig. 5, the *J–V* characteristic curves of devices based on **PCBM** and **BFA** and **BFG** are presented, with a summary of their photovoltaic performance in Table 1. Pristine devices of **BFG** and **BFA** demonstrate comparable short-circuit current densities (J_{sc}) and open-circuit voltages (V_{oc}) to **PCBM**-based devices. However, a significant distinction lies in the fill factor (FF) of **BFG** and **BFA**-based devices, ranging from 0.36 to 0.38, while **PCBM**-based devices achieve an FF of 0.79.

The high resistance observed in **BFG** and **BFA** devices might be attributed to factors beyond the simple presence of dense intermolecular π–π stacking. While π–π stacking often facilitates charge transport, as shown by Ma *et al.*[58] and Zheng *et al.*,[59] who demonstrated that stronger π–π stacking can enhance conductivity and PCE in systems. In some cases, π–π stacking can introduce disorder between domains, leading to reduced charge transport properties.[60] This might explain why the conductivity

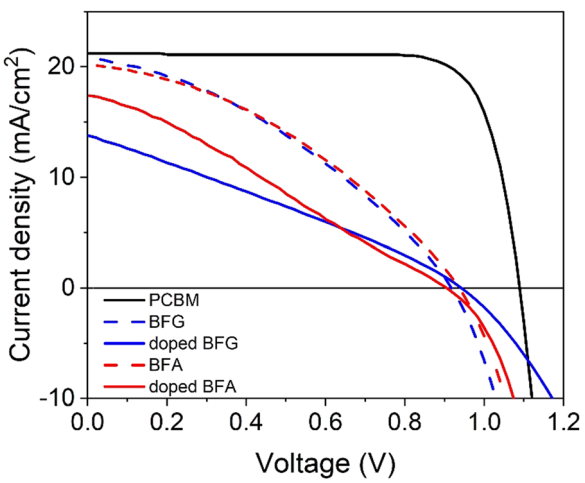

Fig. 5 *J–V* characteristics curves of **PCBM**, undoped and doped of **BFA** and **BFG**-based PSCs.

Table 1 Photovoltaic parameters of reference **PCBM**-based, **BFG**-based and **BFA**-based PSCs

ETL	N-DMBI (mol%)	J_{sc} (mA cm^{-2})	V_{oc} (V)	FF	PCE (%)
PCBM	—	21.19 ± 0.16	1.09 ± 0.00	0.79 ± 0.02	18.26 ± 0.45
BFG	0	20.81 ± 0.42	0.92 ± 0.03	0.36 ± 0.01	6.95 ± 0.48
	20	13.82 ± 1.08	0.94 ± 0.10	0.28 ± 0.00	3.69 ± 0.16
BFA	0	20.22 ± 0.58	0.94 ± 0.14	0.38 ± 0.02	7.11 ± 1.19
	20	17.45 ± 1.22	0.91 ± 0.07	0.28 ± 0.02	4.38 ± 0.34

in the pristine state is low. We note the lower conductivity of the flavin derivatives reported here, especially in comparison to **PCBM**. While **PCBM** increases the conductivity significantly with self-doping upon air exposure from 6.75×10^{-8} S cm^{-1} to 1.58×10^{-6} S cm^{-1} (Fig. S17, ESI†), the flavin derivatives reported here lack the ability to undergo dopant-based doping or self-doping, resulting in higher resistance and lower overall device performance. The film morphology was examined *via* SEM. No significant morphological differences were found between **PCBM**, pristine **BFG** and **BFA**, as show in Fig. S13 (ESI†). Thus, the high resistance in **BFA** and **BFG** devices is more likely linked to their intrinsic low conductivity rather than solely to their π–π stacking behavior.[17,36,54]

Similarly to the lack of charge transport enhancement extracted from the conductivity measurements, the addition of dopant also did not improve the performance of the fabricated solar cells. Indeed, devices incorporating both **BFA** and **BFG** that include the dopant further confirmed the conductivity results. In particular, the addition of the dopant did not increase the performance but rather led to a reduction in the power conversion efficiency, as compared to their pristine counterparts. Here, although the V_{oc} remained constant at around 0.9 V for both undoped and doped devices, the J_{sc} of the doped devices decreased from 20.81 mA cm^{-2} for undoped **BFG** and 20.22 mA cm^{-2} for undoped **BFA** to 13.82 mA cm^{-2} for doped **BFG** and 17.45 mA cm^{-2} for doped **BFA**, respectively. The FF further dropped from 0.36–0.38 in undoped devices to 0.28 in doped devices. This decrease might attributed to the addition of **N-DMBI**, leading to reduced J_{sc} and FF.[36,61] Upon introducing **N-DMBI**, we observe formation of needle shape features as shown in the SEM (Fig. S13, ESI†). The dopant may influence the molecular packing or induce aggregation in the system, similar to behaviours observed in systems with **PCBM**[36,61] and naphthalenediimide,[62] which form large aggregates. This additional loss is likely a result of traps introduced by the dopant[63] that lead to an increase in the recombination of charge carriers and consequent loss in device performance.

It is puzzling that the addition of the dopant, although resulting in a clear radical anion formation as conclusively shown by EPR measurements, does not lead to an increase in conductivity of the film. To understand why this may be the case, we explore the hypothesis that an alternative charged species, *i.e.* a charge-transfer complex (CTC), rather than the free radical is formed instead. Critically, if the generated electron is more likely to stay in the complex than to transfer to an adjacent neutral flavin molecule, then doping would be

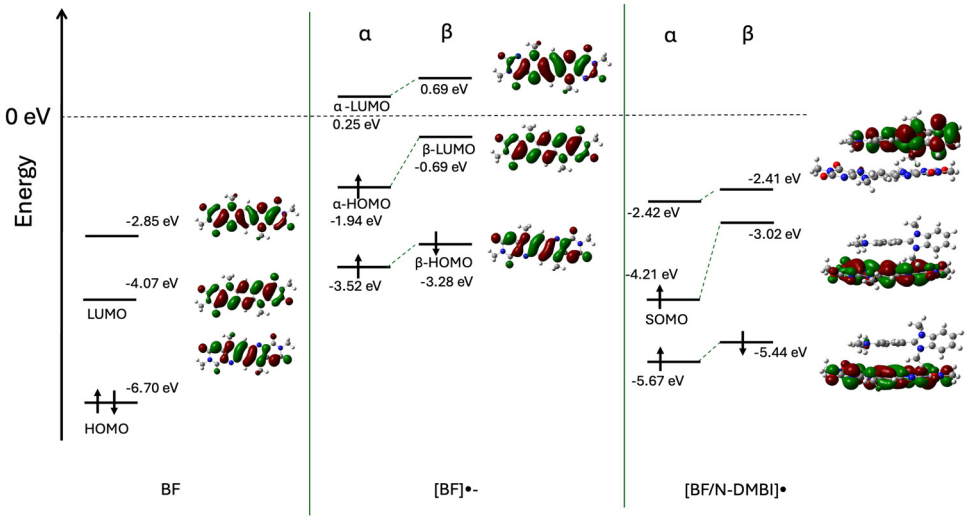

Fig. 6 DFT predicted HOMO/LUMO maps and energies of **BF**, [**BF**$^{\bullet-}$] and **[BF/N-DMBI]**$^{\bullet}$.

unsuccessful as generation of free, *i.e.* unbound, electrons is necessary to increase the conductivity of the films.

To identify whether a charge transfer complex is formed, it is useful to study its energy levels. The energy associated with excitation of a CTC can be determined using the relationship[64]

$$E_e = IP_{donor} - EA_{acceptor} - W$$

where IP_{donor} and $EA_{acceptor}$ are the ionization potential of the donor and the electron affinity of the acceptor, respectively. W is coulombic attraction energy of the complex. Experimentally, E_e was found to follow the relationship[64]

$$E_e\ (eV) = E_{1/2}^{donor} - E_{1/2}^{acceptor} + 0.15$$

Here, $E_{1/2}^{donor}$ and $E_{1/2}^{acceptor}$ are the half-wave electrochemical potentials of the donor and acceptor, respectively. From the CV measurements presented in Fig. 1b, we can estimate E_e to be ~1.96–1.99 eV for a **BFG**/**BFA** complex with **N-DMBI**, corresponding to an absorption feature around 630 nm. Our UV-vis data, as shown in Fig. 3, shows an emerging absorption feature around 675 nm which corresponds to ~1.85 eV. This is broadly within the error estimated to produce the expression above.[64]

To further strengthen this hypothesis, we performed DFT calculations on the radical anion [**BF**$^{\bullet-}$] and its complex with **N-DMBI** [**BF/N-DMBI**] (Fig. 6 and ESI†). The spin density map of the [**BF**$^{\bullet-}$] reveals that the radical is highly delocalised throughout the acceptor core suggesting a stabilised radical is formed (ESI†). The calculated LUMO level of **BF** (−4.07 eV) are significantly offset from the SOMO of **[BF/N-DMBI]**$^{\bullet}$ (−4.21 eV), indicating that it is energetically unfavourable for an electron of the complex to be transferred to a neutral **BF** unit. Additionally, the calculated LUMO level of **BF** is significantly offset from the SOMOs of **BF**$^{\bullet-}$ (−1.94 eV) and **N-DMBI**. (−2.51 eV) and the HOMO of **N-DMBI** (−4.37 eV) which could also contribute to the low conductivity observed.[52,65]

The predicted UV-vis spectra from TD-DFT calculations performed on **[BF/N-DMBI]**$^{\bullet}$ (Fig. 7) further suggest CTC formation. When this spectrum is compared to the experimentally obtained spectra for **[BF/N-DMBI]**$^{\bullet}$, similar spectral features were observed (ESI†). In particular, solution UV-vis spectra give rise to new absorptions at 675 nm and 1022 nm upon addition of the dopant, whereas the TD-DFT predicted UV-vis gave peaks at 644 nm and 868 nm (Fig. S16, ESI†). This was further supported when the electrostatic potentials (ESPs) (Fig. 7a) of the complex were investigated which revealed positive ESPs for the dopant and negative ESPs for the acceptor, with the negative charge being localised on the more electronegative oxygen and nitrogen atoms of the latter. The spin density maps of the complex indicated that the radical is highly delocalised on the **BF** unit (Fig. 7b). Mulliken charge population analysis performed on **[BF/N-DMBI]**$^{\bullet}$ indicated a high degree of charge transfer between the components of the complex (0.9e).[50] Lastly, the calculated binding energies of **[BF/N-DMBI]**$^{\bullet}$ and the π–π dimer of **BF** (**BF/BF**), revealed that former was significantly stronger (E_b = −53.1 *versus* −6.9 kcal mol^{-1}). The greater strength of the CT complex will lead to a significant decrease in electron mobility in films due to the disruption of long range π–π stacking (Fig. 8).

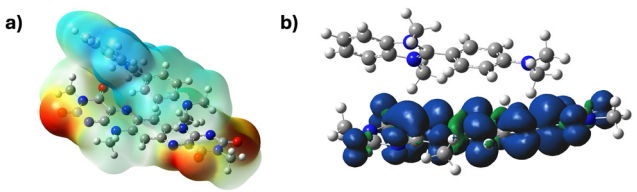

Fig. 7 (a) ESP and (b) spin density maps of **[BF/N-DMBI]**$^{\bullet}$.

Conclusions

This study has investigated the potential of bioinspired derivatives **BFG** and **BFA** as ETMs for PSCs. Pristine devices of **BFG** and **BFA** exhibit promising photovoltaic performance, achieving approximately 7% PCEs with competitive J_{sc} and V_{oc} values.

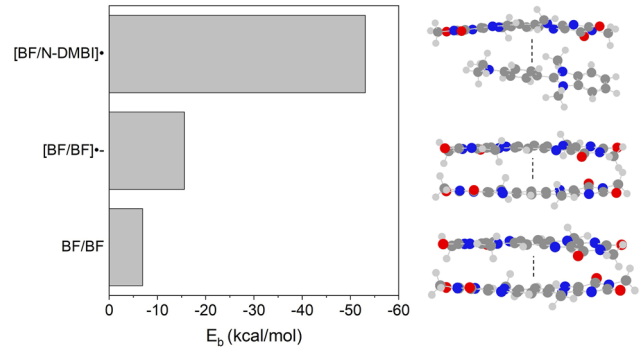

Fig. 8 Calculated binding energies for **[BF/N-DMBI]•** and **BF/BF**.

This suggests that these derivatives have potential as an n-type organic material for ETL applications in photovoltaics. The study also delves into the n-type doping of these derivatives, revealing distinct doping behaviours between the glycol and alkyl side chain functionalised systems. Glycol-functionalized **BFG** shows faster reactivity with the n-type dopant **N-DMBI**, achieving the maximum quantity of reduced species in a shorter reaction time compared to **BFA**. However, solar cells incorporating this dopant show no enhancement mainly due to the lack of improvement in charge transport, as conclusively shown through conductivity measurements. DFT modelling has indicated that these materials tend to form stable CTCs in the doping process and that electron transfer between the SOMO of the **N-DMBI** and **BFA/BFG** complex and the LUMO of a **BFA/BFG** moiety is energetically unfavourable and consequently an electron is unlikely to be donated to the matrix of surrounding undoped molecules. Therefore, our results indicate that doping with **N-DMBI** is not an effective strategy for these systems and that charge-transfer complexation may prevent effective n-doping. As organic electron deficient materials are important components in a range of technologies including optoelectronic (*e.g.* solar cells. OLEDs) and thermoelectric devices, this work thereby highlights the importance of utilising relatively low-cost DFT calculations early in the design process of new electron deficient materials and their dopants.

Data availability

The ESI,† includes the data described in this manuscript including: synthetic protocols, new molecule characterisation, theoretical calculation information and device fabrication and characterisation information and protocols.

Conflicts of interest

There are no conflicts of interests.

Acknowledgements

WKY thanks the University of Glasgow for a College of Science and Engineering PhD scholarship. GC thanks the EPSRC (EP/E036244/1) and the Leverhulme Trust for a Research Fellowship. PD would like to thank the EPSRC for funding (EP/T010568/1).

References

1 Y.-C. Wang, X. Li, L. Zhu, X. Liu, W. Zhang and J. Fang, *Adv. Energy Mater.*, 2017, **7**, 1701144.
2 R. Sandoval-Torrientes, J. Pascual, I. García-Benito, S. Collavini, I. Kosta, R. Tena-Zaera, N. Martín and J. L. Delgado, *ChemSusChem*, 2017, **10**, 2023–2029.
3 F. Zhang, W. Shi, J. Luo, N. Pellet, C. Yi, X. Li, X. Zhao, T. J. S. Dennis, X. Li, S. Wang, Y. Xiao, S. M. Zakeeruddin, D. Bi and M. Grätzel, *Adv. Mater.*, 2017, **29**, 1606806.
4 O. V. Kharissova, B. I. Kharisov, C. Máximo, O. González, Y. Peña Méndez and I. López, *R. Soc. Open Sci.*, 2019, **6**, 191378.
5 P. Pimviriyakul and P. Chaiyen, *Enzymes*, 2020, **47**, 1–36.
6 E. C. Breinlinger, C. J. Keenan and V. M. Rotello, *J. Am. Chem. Soc.*, 1998, **120**, 8606–8609.
7 Y. M. Legrand, M. Gray, G. Cooke and V. M. Rotello, *J. Am. Chem. Soc.*, 2003, **125**, 15789–15795.
8 A. M. Edwards, *Flavins and Flavoproteins: Methods and Protocols*, 2014.
9 C. Dalal and N. R. Jana, *Langmuir*, 2019, **35**, 11380–11388.
10 S. Feng, F. Pei, Y. Wu, J. Lv, Q. Hao, T. Yang, Z. Tong and W. Lei, *Spectrochim. Acta, Part A*, 2021, **246**, 119004.
11 S. Alonso-de Castro, A. Terenzi, S. Hager, B. Englinger, A. Faraone, C. Martínez, K. Keppler, W. Berger, L. Salassa and M. Sophia, *Sci. Rep.*, 2018, **8**, 17198.
12 T. Morack, J. B. Metternich and R. Gilmour, *Org. Lett.*, 2018, **20**, 1316–1319.
13 X. Yu, S. Eymur, V. Singh, B. Yang, M. Tonga, A. Bheemaraju, G. Cooke, C. Subramani, D. Venkataraman, R. J. Stanley and V. M. Rotello, *Phys. Chem. Chem. Phys.*, 2012, **14**, 6749–6754.
14 W. Brütting and C. Adachi, *Physics of Organic Semiconductors*, Wiley-VCH Verlag GmbH & Co. KGaA, 2005.
15 K. Pei, *Surf. Interfaces*, 2022, **30**, 101887.
16 J. Lian, B. Lu, F. Niu, P. Zeng and X. Zhan, *Small Methods*, 2018, **2**, 1800082.
17 L. Hu, T. Liu, J. Duan, X. Ma, C. Ge, Y. Jiang, F. Qin, S. Xiong, F. Jiang, B. Hu, X. Gao, Y. Yi and Y. Zhou, *Adv. Funct. Mater.*, 2017, **27**, 1703254.
18 Z. Wang, D. P. McMeekin, N. Sakai, S. van Reenen, K. Wojciechowski, J. B. Patel, M. B. Johnston and H. J. Snaith, *Adv. Mater.*, 2017, **29**, 1604186.
19 Q. Q. Ye, Z. K. Wang, M. Li, C. C. Zhang, K. H. Hu and L. S. Liao, *ACS Energy Lett.*, 2018, **3**, 875–882.
20 X. Zhao, D. Madan, Y. Cheng, J. Zhou, H. Li, S. M. Thon, A. E. Bragg, M. E. DeCoster, P. E. Hopkins and H. E. Katz, *Adv. Mater.*, 2017, **29**, 1606928.
21 C. Geffroy, E. Grana, T. Bessho, S. Almosni, Z. Tang, A. Sharma, T. Kinoshita, F. Awai, E. Cloutet, T. Toupance, H. Segawa and G. Hadziioannou, *ACS Appl. Energy Mater.*, 2020, **3**, 1393–1401.

22 D.-Y. Chen, W.-H. Tseng, S.-P. Liang, C.-I. Wu, C.-W. Hsu, Y. Chi, W.-Y. Hung and P.-T. Chou, *Phys. Chem. Chem. Phys.*, 2012, **14**, 11689–11694.
23 T. Ye, J. Wang, W. Chen, Y. Yang and D. He, *ACS Appl. Mater. Interfaces*, 2017, **9**, 17923–17931.
24 J. Burschka, A. Dualeh, F. Kessler, E. Baranoff, N. L. Cevey-Ha, C. Yi, M. K. Nazeeruddin and M. Grätzel, *J. Am. Chem. Soc.*, 2011, **133**, 18042–18045.
25 I. E. Jacobs and A. J. Moulé, *Adv. Mater.*, 2017, **29**, 1703063.
26 H. Xia, M. Zhang, H. Wang, Y. Sun, Z. Li, R. Ma, H. Liu, T. A. Dela Peña, H. T. Chandran, M. Li, J. Wu, X. Lu, W. Y. Wong and G. Li, *Adv. Funct. Mater.*, 2024, 2411058.
27 Y. Xu, H. Sun, A. Liu, H. H. Zhu, W. Li, Y. F. Lin and Y. Y. Noh, *Adv. Mater.*, 2018, **30**, 1801830.
28 K. Pei, A. Ho, Y. Lau, P. Kwok and L. Chan, *Phys. Chem. Chem. Phys.*, 2020, **22**, 7100–7109.
29 Z.-C. Wen, H. Yin and X.-T. Hao, *Surf. Interfaces*, 2021, **23**, 100921.
30 H.-T. Chien, M. Pölzl, G. Koller, S. Challinger, C. Fairbairn, I. Baikie, M. Kratzer, C. Teichert and B. Friedel, *Surf. Interfaces*, 2016, **6**, 72–80.
31 Y. Liu, B. Nell, K. Ortstein, Z. Wu, Y. Karpov, T. Beryozkina, S. Lenk, A. Kiriy, K. Leo and S. Reineke, *ACS Appl. Mater. Interfaces*, 2019, **11**, 11660–11666.
32 X. Lin, B. Wegner, K. M. Lee, M. A. Fusella, F. Zhang, K. Moudgil, B. P. Rand, S. Barlow, S. R. Marder, N. Koch and A. Kahn, *Nat. Mater.*, 2017, **16**, 1209–1215.
33 W. Zhao, J. Ding, Y. Zou, C. A. Di and D. Zhu, *Chem. Soc. Rev.*, 2020, **49**, 7210–7228.
34 E. Hyun Suh, Y. Jin Jeong, J. Gyu Oh, K. Lee, J. Jung, Y. Soo Kang and J. Jang, *Nano Energy*, 2019, **58**, 585–595.
35 T. H. Kim, J. H. Kim and K. Kang, *Jpn. J. Appl. Phys.*, 2023, **62**, SE0803.
36 S. Kim, S. Bae and H. Jo, *Chem. Commun.*, 2015, **51**, 17413.
37 Z. Bin, J. Li, L. Wang and L. Duan, *Energy Environ. Sci.*, 2016, **9**, 3424–3428.
38 F. Galatopoulos, S. Bitton, M. Tziampou, N. Tessler and S. A. Choulis, *ACS Appl. Electron. Mater.*, 2023, **5**, 5580–5587.
39 J. Liu, M. P. Garman, J. Dong, B. Van Der Zee, L. Qiu, G. Portale, J. C. Hummelen and L. J. A. Koster, *ACS Appl. Energy Mater.*, 2019, **2**, 6664–6671.
40 J. Liu, L. Qiu, G. Portale, S. Torabi, M. C. A. Stuart, X. Qiu, M. Koopmans, R. C. Chiechi, J. C. Hummelen, L. Jan and A. Koster, *Nano Energy*, 2018, **52**, 183–191.
41 J. Dong, S. Sami, D. M. Balazs, R. Alessandri, F. Jahani, L. Qiu, S. J. Marrink, R. W. A. Havenith, J. C. Hummelen, M. A. Loi and G. Portale, *J. Mater. Chem. C*, 2021, **9**, 16225.
42 A. Fakharuddin, K. K. Armadorou, L. P. Zorba, M. Tountas, T. Seewald, A. Soultati, P. Tsipas, E. R. Schütz, N. Tzoganakis, S. Panagiotakis, K. Yannakopoulou, A. Dimoulas, V. Psycharis, E. Kymakis, A. R. bin, M. Yusoff, K. Aidinis, L. Schmidt-Mende, G. C. Vougioukalakis, M. K. Nazeeruddin and M. Vasilopoulou, *Chin. J. Chem.*, 2023, **41**, 431–442.
43 M. Lenes, G. J. A. H. Wetzelaer, F. B. Kooistra, S. C. Veenstra, J. C. Hummelen and P. W. M. Blom, *Adv. Mater.*, 2008, **20**, 2116–2119.
44 Y. Shao, Y. Yuan and J. Huang, *Nat. Energy*, 2016, **1**, 15001.
45 J. Y. Jeng, Y. F. Chiang, M. H. Lee, S. R. Peng, T. F. Guo, P. Chen and T. C. Wen, *Adv. Mater.*, 2013, **25**, 3727–3732.
46 L. Zhou, J. Chang, Z. Liu, X. Sun, Z. Lin, D. Chen, C. Zhang, J. Zhang and Y. Hao, *Nanoscale*, 2018, **10**, 3053.
47 P. Wei, J. H. Oh, G. Dong and Z. Bao, *J. Am. Chem. Soc.*, 2010, **132**, 8852–8853.
48 D. D. Tanner, J. J. Chen, L. Chen and C. Luelo, *J. Am. Chem. Soc.*, 1991, **113**, 8074–8081.
49 D. D. Tanner and J. J. Chen, *J. Org. Chem.*, 1989, **54**, 3842–3846.
50 Y. Zeng, W. Zheng, Y. Guo, G. Han and Y. Yi, *J. Mater. Chem. A*, 2020, **8**, 8323–8328.
51 O. Bardagot, C. Aumaître, A. Monmagnon, J. Pécaut, P. A. Bayle and R. Demadrille, *Appl. Phys. Lett.*, 2021, **118**, 203904.
52 S. Riera-Galindo, A. Orbelli Biroli, A. Forni, Y. Puttisong, F. Tessore, M. Pizzotti, E. Pavlopoulou, E. Solano, S. Wang, G. Wang, T. P. Ruoko, W. M. Chen, M. Kemerink, M. Berggren, G. Di Carlo and S. Fabiano, *ACS Appl. Mater. Interfaces*, 2019, **11**, 37981–37990.
53 Y. Yano, M. Nakazato, K. Lizuka, T. Hoshino, K. Tanaka, M. Kogab and F. Yoneda, *J. Chem. Soc., Perkin Trans. 2*, 1990, 2179–2185.
54 J. Li, F. Qin, W. Zeng, L. Sun, W. Wang and Y. Zhou, *Sustainable Energy Fuels*, 2020, **4**, 1984–1990.
55 Z. Wang, D. P. McMeekin, N. Sakai, S. van Reenen, K. Wojciechowski, J. B. Patel, M. B. Johnston and H. J. Snaith, *Adv. Mater.*, 2017, **29**, 1604186.
56 X. Liu, P. Li, Y. Zhang, X. Hu, Y. Duan, F. Li, D. Li, G. Shao and Y. Song, *J. Power Sources*, 2019, **413**, 459–466.
57 M. Koopmans, M. A. T. Leiviskä, J. Liu, J. Dong, L. Qiu, J. C. Hummelen, G. Portale, M. C. Heiber and L. J. A. Koster, *ACS Appl. Mater. Interfaces*, 2020, **12**, 56222–56230.
58 Q. Ma, J. Qiu, Y. Yang, F. Tang, Y. Zeng, N. Ma, B. Yu, F. Lu, C. Liu, A. Lambertz, W. Duan, K. Ding and Y. Mai, *J. Energy Chem.*, 2023, **82**, 25–30.
59 A. Zheng, J. Wang, N. Xu, R. Zhu, Y. Yuan, J. Zhang, J. Zhang, Z. Li and P. Wang, *ACS Photonics*, 2018, **5**, 4694–4701.
60 B. Vella, M. H. Fsadni, T. Pope, M. Giza, F. J. Angus, I. Shmarov, P. L. Lalaguna, M. Cariello, C. Wilson, M. Kadodwala, T. J. Penfold, P. Docampo and G. Cooke, *J. Mater. Chem. A*, 2024, **12**, 22844–22858.
61 J. H. Bae, Y. J. Noh, M. Kang, D. Y. Kim, H. Bin Kim, S. H. Oh, J. M. Yun and S. I. Na, *RSC Adv.*, 2016, **6**, 64962–64966.
62 D. Kiefer, A. Giovannitti, H. Sun, T. Biskup, A. Hofmann, M. Koopmans, C. Cendra, S. Weber, L. J. Anton Koster, E. Olsson, J. Rivnay, S. Fabiano, I. McCulloch and C. Müller, *ACS Energy Lett.*, 2018, **3**, 278–285.
63 M. N. Le, H. Kim, B. Yeo, K. Kang, Y. Song, X. Guo, Y.-G. Ha, C. Kim and M.-G. Kim, *J. Mater. Chem. C*, 2019, **7**, 10635–10641.
64 M. S. A. Abdou, F. P. Orfino, Y. Son and S. Holdcroft, *J. Am. Chem. Soc.*, 1997, **119**, 4518–4524.
65 D. Yuan, D. Huang, C. Zhang, Y. Zou, C. A. Di, X. Zhu and D. Zhu, *ACS Appl. Mater. Interfaces*, 2017, **9**, 28795–28801.